Rupture details of the 28 March 2005 Sumatra M*w* 8.6 earthquake imaged with teleseismic *P* waves

Kristoffer T. Walker, Miaki Ishii, and Peter M. Shearer

Institute of Geophysics and Planetary Physics, Scripps Institution of Oceanography, University of California, San Diego, USA

Received 18 August 2005; revised 26 October 2005; accepted 3 November 2005; published 20 December 2005.

[1] We image the rupture of the 28 March 2005 Sumatra M*w* 8.6 earthquake by back-projecting teleseismic *P* waves recorded by the Global Seismic Network and the Japanese Hi-net to their source. The back-projected energy suggests that the rupture started slowly, had a total duration of about 120 s, and propagated at 2.9 to 3.3 km/s from the hypocenter in two different directions: first toward the north for ~100 km and then, after a ~40 s delay, toward the southeast for ~200 km. Our images are consistent with a rupture area of ~40,000 km^2, the locations of the first day of aftershocks, and the Harvard CMT M*w* of 8.6, which implies an average slip of ~6 m. The earthquake is similar in its location, size, and geometry to a M*w* ~8.5 event in 1861. Our estimated average slip is consistent with a partially coupled subduction interface, GPS forearc velocities, and the ~59 mm/yr convergence rate if the 2005 earthquake released elastic strain that accumulated over many hundreds of years rather than just since the last 1861 event. **Citation:** Walker, K. T., M. Ishii, and P. M. Shearer (2005), Rupture details of the 28 March 2005 Sumatra M*w* 8.6 earthquake imaged with teleseismic *P* waves, *Geophys. Res. Lett.*, *32*, L24303, doi:10.1029/2005GL024395.

1. Introduction

[2] On 26 December 2004, a subduction zone earthquake estimated at M*w* 9.3 [*Stein and Okal*, 2005] struck off the coast of northern Sumatra. The rupture propagated unilaterally to the north for over 1200 km to the Andaman Islands [*Ishii et al.*, 2005]. Seismic shaking and a large tsunami inflicted catastrophic damage with an estimated 300,000 casualties throughout the region and in coastal areas around the Indian Ocean. A second thrust event of M*w* 8.6 occurred on 28 March 2005, about 300 km to the east-southeast of the M*w* 9.3 epicenter (Figure 1). The resulting tsunami was much smaller and largely focused away from civilization toward the southern Indian Ocean. However, the surface shaking resulted in ~2000 casualties, most of which occurred in collapsed houses on the nearby island of Nias.

[3] We apply a *P*-wave back-projection method to image rupture details of the March 2005 earthquake. We have previously used this approach in imaging the 2004 Sumatra-Andaman earthquake using data from the Japanese High Sensitivity Seismograph Network (Hi-net [*Ishii et al.*, 2005]). Here we show that the method is also effective in resolving rupture details of the March 2005 earthquake using seismograms from the Global Seismic Network as well as the Hi-net. Specifically, we resolve a 120-s long, bilateral rupture, with the initial rupture propagating northward, followed by a second larger area of slip propagating to the southeast from the hypocenter. We use our images, together with focal mechanisms, moment estimates, and aftershock locations to infer the distribution of fault slip. We then compare our results with other geophysical data to evaluate the nature of slab-plate coupling.

0094-8276/05/2005GL024395$05.00

2. Study Area

[4] The Indo-Australian plate is subducting beneath northern Sumatra at 59 ± 5 mm/yr at an oblique angle to the margin (velocities computed using plate-velocity models available at http://sps.unavco.org) (Figure 1). The Great Sumatran Fault is located on land and accommodates right-lateral, strike-slip motion (24 ± 4 mm/yr), while the subduction zone accommodates dip-slip motion offshore (42 ± 4 mm/yr [*Genrich et al.*, 2000; *McCaffrey et al.*, 2000]). The Benioff zone dips at ~15° at shallow depths beneath the outer arc rise and at ~50° at deeper depths beneath the volcanic arc [*Fauzi et al.*, 1996].

[5] Two thrust earthquakes (M*w* ~8.5 and M*w* ~8.8) occurred in 1861 and 1833 near Nias Island and southwest of Siberut Island, respectively (Figure 1) [*Newcomb and McCann*, 1987; *Zachariasen et al.*, 1999; *Rivera et al.*, 2002; *Natawidjaja et al.*, 2004]. An area of enhanced seismicity exists between the 1861 and 1833 ruptures along the subducting north-trending Investigator Fracture Zone [*Fauzi et al.*, 1996; *Rivera et al.*, 2002]. Paleogeodetic records of vertical deformation from coral microatolls in the area, where the fracture zone impinges upon the margin, suggest that the subduction zone has been at least partially locked above depths of 30 km during 1970–1997 [*Sieh et al.*, 1999]. GPS-determined forearc velocities suggest an abrupt change in forearc deformation at the fracture zone, between a mostly locked zone toward the southeast and a partially locked zone to the northwest [*Prawirodirdjo et al.*, 1997].

3. Methodology

[6] The *P* wavetrain of a large earthquake is generated by the temporal-spatial distribution of fault slip, with a slip patch moving in the direction(s) of rupture propagation. The first-arriving energy comes from the hypocenter, whereas later-arriving energy is due to slip at and behind the rupture front. Using the method described by *Ishii et al.* [2005], we back-project *P* waves to potential source locations. In map view as a function of reverse time, the back-projected energy for a single station appears as a series of expanding circles centered above the seismic station. Back-projected

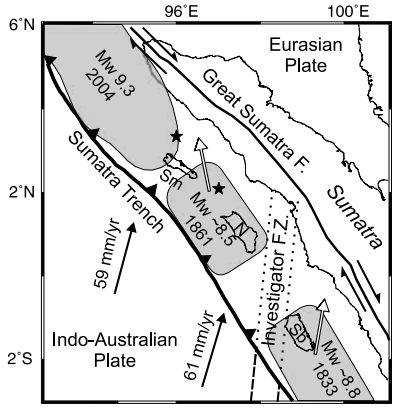

Figure 1. Study area showing the areas of past large subduction zone earthquakes. Rupture areas of 1861 and 1833 events are constrained by historical records and coral microatoll data, but the exact boundaries are not well known [*Newcomb and McCann*, 1987; *Zachariasen et al.*, 1999; *Rivera et al.*, 2002; *Natawidjaja et al.*, 2004]. The area for the 2004 Sumatra-Andaman event is obtained from *Ishii et al.* [2005]. Black stars: USGS epicenter locations for the 2004 and 2005 earthquakes. Islands: Nias (N), Siberut (Sb), and Simeuleue (Sm). Black arrow: plate convergence direction. White arrows: average direction of GPS-derived forearc velocities.

energy from stations in different locations constructively interferes at the source and destructively interferes elsewhere. These stacked images, S(**x**, t) where **x** is the position of the potential source location (x, y, z) and t is the time with respect to the onset time, provide an estimate of the relative intensity of *P*-wave radiation in the rupture zone. Because teleseismic *P*-wave travel times provide poor constraints on source depth, we only back-project to source locations as a function of latitude and longitude at the hypocenter depth (S(x, y, t)).

[7] We use a 1D velocity model (IASP91 [*Kennett and Engdahl*, 1991]) to predict travel times. *P*-wave travel-time deviations due to 3D structure are typically less than 3 s, but can significantly degrade the coherence. We correct for these deviations by aligning the initial *P* arrivals using an iterative, multi-station cross-correlation technique [*Reif et al.*, 2002], which provides measures of waveform similarity (the correlation coefficient), polarities, and optimum time shifts (Figure 2).

4. Results

[8] We back-project seismograms recorded by stations of the broadband Global Seismic Network (GSN) and short-period Japanese Hi-net (Figure 3a). The GSN waveforms sorted by source-to-station azimuth generally show weak amplitudes within the first 15 s (Figure 2). The arrivals within the first 30 s for stations with SW-SE azimuths are exceptionally weak, suggesting an initial rupture direction toward the north.

[9] For the GSN stations, the similarity coefficient of the initial 5 s of the *P* wavetrain with the stack ranges from 0.77 to 0.99. The traces are allowed to shift by up to ±10 s, but the optimum shifts are between −2 and 8 s. To minimize the effect of a misaligned seismogram on the back projection due to adverse effects of directivity and propagation along a nodal plane, we assume a maximum time shift threshold of 3 s. Using a time-varying amplitude normalization prior to the cross-correlation reduces these adverse effects (available in the auxiliary material[1]) and decreases the number of stations with time shifts of more than 3 s from 9 to 4. The remaining 4 stations have east to southeast azimuths and are discarded.

[10] Our images integrated over the 120-s duration of the rupture are shown in Figure 3. The GSN and Hi-net seismograms generally illuminate a rupture zone mostly southeast of the epicenter (Figures 3b and 3c). Comparing the first and second halves of the rupture, Figures 3d and 3e show that the rupture propagated toward the north initially, followed by propagation toward the southeast. The distance from the epicenter to centroids of time-integrated S(x, y) (computed using the 90% contour of the maximum value in 5 s increments) also suggests a delayed, bilateral rupture that propagated at about 2.9 to 3.3 km/s (Figure 3f). The first 15 s of the rupture is difficult to track because of the weak amplitudes. However, it appears that the rupture propagated slowly from the hypocenter, and picked up speed ~15 s later. Significant southeastern propagation did not begin until ~40 s after the onset of the rupture.

[11] We estimate source-time functions using the GSN and Hi-net waveforms by plotting the stack amplitude at high-quality centroids as a function of time (see the auxiliary material). Both the GSN and Hi-net functions have weak amplitudes during the first 15 s, and a peak at ~75 s. However, the Hi-net function suggests a ~90 s duration whereas the GSN function suggests ~120 s. In addition, the first 30 s of the GSN function is higher in relative amplitude than that of the Hi-net. By back-projecting GSN waveforms in different frequency bands, we find considerable differ-

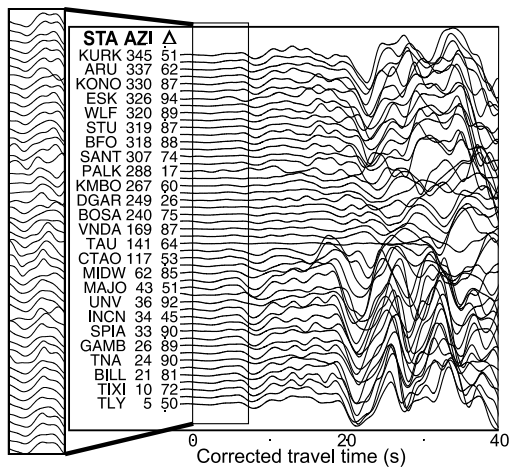

Figure 2. GSN waveforms aligned and sorted by source-to-station azimuth. The onset of the *P* wavetrain begins at 0 s. The waveforms within the first 7.5 s (left panel) correspond to the energy originating from the hypocenter. The coherence degrades with time because the rupture propagates to different locations. Only every other seismogram is labeled.

[1]Auxiliary material is available at ftp://ftp.agu.org/apend/gl/2005GL024395.

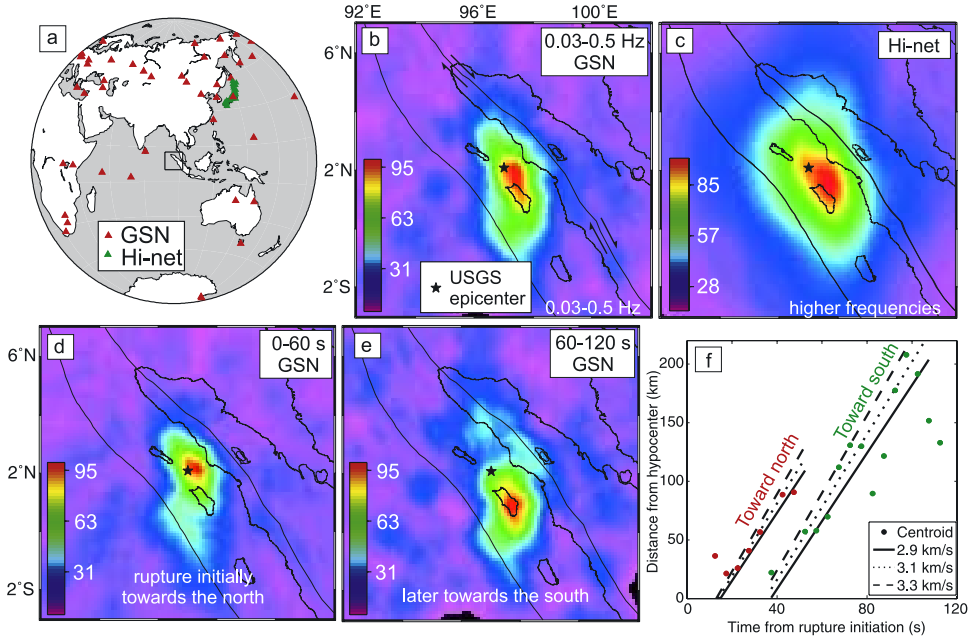

Figure 3. Images of the back-projected *P* waves. Stations from the Global Seismic Network (GSN) and Japanese Hi-net are used in this study (a). The maximum-normalized (to 100), time-integration of S(x, y, t) for the entire rupture (b–c) and the first and second halves of the rupture (d–e), with warm colors indicating high seismic energy.

ences in the relative amplitudes and timings of the estimated source-time functions.

5. Discussion

[12] The focal mechanisms based on the first-arriving *P* waves (USGS) and surface waves (Harvard CMT) for the 2005 Sumatra event suggests that it occurred along a subhorizontal thrust fault (Figure 4). We therefore interpret our distribution of back-projected energy as the ruptured fault plane, and base our interpretations on the GSN image because experiments suggest it has better resolution than the Hi-net image[2]. However, it is difficult to determine the limits of the fault plane from this image alone (Figure 4) because it does not have a clearly defined edge. Consequently, we calibrate our results using independent estimates of the fault area. An area of ~40,000 km^2 is roughly consistent with the region spanned by the first day of aftershocks, as well as the empirical relationship between earthquake rupture areas and moment for a M*w* 8.6 earthquake [*Abe*, 1975; *Geller and Kanamori*, 1977]. We select the 58% contour in our time-integrated image, corresponding to an area of 40,000 km^2 as the rupture boundary. This rupture area is not coincident with aftershocks to the northwest near Simeuleue Island, the region connecting our imaged rupture to that of the 2004 M*w* 9.3 earthquake. We can choose successively lower contours to include more of these aftershocks, but this quickly increases the surface area to 70,000 km^2, which is more consistent with M*w* 8.8. We prefer the conservative estimate of 40,000 km^2, and interpret the aftershocks in the northwest to be triggered by the mainshock and perhaps promoted by the 2004 M*w* 9.3 event. Assuming a rigidity of 42 GPa [*Bilek and Lay*, 1999], we calculate an average slip of 5.9 m.

[13] If we assume a linear relationship between energy and fault slip, we can use the imaged energy distribution (normalized to zero at the 58% contour) to estimate the slip distribution (Figure 4). This distribution is highly dependent upon the smoothing imposed by the resolution kernel; for example, it would be significantly smaller if the energy ended more abruptly at the rupture boundary (see the auxiliary material).

[14] One might expect the Harvard CMT and the centroid of our rupture image to be collocated. However, the CMT is located ~50 km to the west of the GSN and Hi-net centroids (Figure 4). The CMT is based on 300–500 s surface waves, which may be sensitive to different features of the rupture process than the higher-frequency *P* waves. We interpret the ~50 km offset as an attribute of the sensitivity and resolution differences between the two methods.

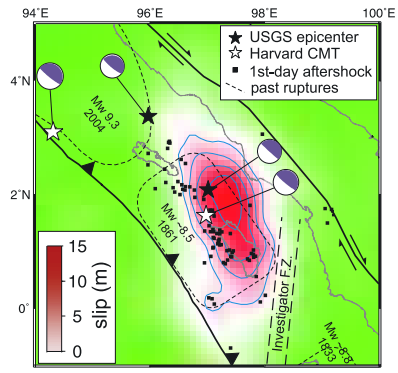

Figure 4. Fault rupture interpretation of the GSN *P*-wave image. Color shows the total slip during the 2005 Sumatra earthquake as estimated from scaling based on empirical relationships (see text). Blue contour line gives the 58% level of the maximum amplitude of S(x,y,t), which is our estimated rupture boundary.

[15] The position of the stack centroids as a function of time suggests a delay of 25 s between the onsets of two separate rupture propagations (Figure 3f). Because the rupture propagation appeared to be slow during the first 15 s, the energy release in the southeastern region started ~40 s after the onset. An alternative interpretation is that the rupture propagated simultaneously away from the hypocenter in both directions, but the seismic radiation was stronger in the north and the rupture propagation was initially slower toward the south only to increase in speed around 40 to 60 s after the onset.

[16] The spatial extents of the 2005 (M*w* 8.6) and 1861 (M*w* ~8.5) ruptures are remarkably similar (Figure 4). No other large earthquakes have occurred along this rupture zone during the interim. If the average slip vector indicated by the Harvard CMT is representative of the entire fault rupture and the subduction zone has been locked, the 42 ± 4 mm/yr trench-normal convergence rate suggests 5.5 to 6.6 m of accumulated elastic strain since 1861, in agreement with our estimated average slip of 5.9 m. However, modeling of 1989–1993 GPS measurements in this region by *Prawirodirdjo et al.* [1997] indicates only about 40% coupling between the forearc and the subducting plate, in which case the accumulated strain since 1861 is reduced to roughly half of our estimated average slip for the 2005 earthquake. There are several possible explanations for the discrepancy between the accumulated strain and the inferred slip: (1) we overestimate the average slip; (2) the rupture is too complicated to be accurately characterized with a single focal mechanism; (3) the subduction zone has been mostly locked since 1861, and the four-year GPS survey measured velocities that are not representative of the 144-year average; or (4) the 2005 event released more strain than that accumulated since the 1861 earthquake. We prefer the last interpretation because of its simplicity and its consistency with the promotion of failure in this region by the neighboring M*w* 9.3 2004 event.

[17] An earthquake of M*w* ~8.8 occurred in 1833 to the southeast of Siberut Island and fracture zone. The trench-normal component of the 44 ± 4 mm/yr convergence rate for well-coupled subduction suggests 7 to 8 m of strain since 1833. If the recent 9.3 and 8.6 events trigger the release of this accumulated strain, it could generate a large earthquake similar to that of 1833, and an even larger earthquake if the earthquake releases more than just the post-1833 accumulated strain in the same fashion as that suggested for the 2005 M*w* 8.6 event to the northwest.

6. Conclusions

[18] Our results for the Sumatra M*w* 8.6 earthquake suggest that the first 15 s of the 120-s rupture is relatively weak and slow, but is followed by what we interpret as a bilateral rupture spanning an area of ~40,000 km^2. The rupture propagation initiates from the hypocenter and proceeds toward the north lasting for ~50 s. A second larger rupture starts at about 40 s from the hypocentral time and propagates toward the southeast. Apparent average rupture speeds in both directions are between 2.9 and 3.3 km/s, which are slightly faster than those found for the Sumatra M*w* 9.3 event [*Ammon et al.*, 2005; *Ishii et al.*, 2005]. The area of our *P*-wave rupture image is generally consistent with the locations of the first day of aftershocks and the Harvard M*w* 8.6. We crudely estimate the slip distribution using simple scaling relationships for large, shallow earthquakes, with an average slip of ~5.9 m. Reconciling this slip with GPS forearc velocities suggests that the 2005 event may have released more than the elastic strain that accumulated since the M*w* ~8.5 earthquake in 1861.

[19] **Acknowledgments.** The seismic data were provided by the National Earthquake Information Center (USGS), Scripps Institution of Oceanography, and the National Research Institute for Earth Science and Disaster Prevention in Japan. We thank S. Bilek for sharing her preliminary slip distribution model with us, and K. Sieh for useful discussions. We also thank G. Beroza and A. Levander for constructive reviews of this manuscript.

References

Abe, K. (1975), Reliable estimation of the seismic moment of large earthquakes, *J. Phys. Earth*, *23*, 381–390.

Ammon, C. J., et al. (2005), Rupture process of the 2004 Sumatra-Andaman earthquake, *Science*, *308*, 1133–1139.

Bilek, S. L., and T. Lay (1999), Rigidity variations with depth along interplate megathrust faults in subduction zones, *Nature*, *400*, 443–446.

Fauzi, , R. McCaffrey, D. Wark, Sunaryo, and P. Y. Prih Haryadi (1996), Lateral variation in slab orientation beneath Toba caldera, northern Sumatra, *Geophys. Res. Lett.*, *23*, 443–446.

Geller, R. J., and H. Kanamori (1977), Magnitude of great shallow earthquakes from 1904 to 1952, *Bull. Seismol. Soc. Am.*, *67*, 587–598.

Genrich, J. F., Y. Bock, R. McCaffrey, L. Prawirodirdjo, C. W. Stevens, S. S. O. Puntodewo, C. Subarya, and S. Wdowinski (2000), Distribution of slip at the northern Sumatran fault system, *J. Geophys. Res.*, *105*, 28,327–28,341.

Ishii, M., P. M. Shearer, H. Houston, and J. E. Vidale (2005), Extent, duration and speed of the 2004 Sumatra-Andaman earthquake imaged by the Hi-net array, *Nature*, *435*, 933–936.

Kennett, B. L. N., and E. R. Engdahl (1991), Traveltimes for global earthquake location and phase identification, *Geophys. J. Int.*, *105*, 429–465.

McCaffrey, R., P. C. Zwick, Y. Bock, L. Prawirodirdjo, J. F. Genrich, C. W. Stevens, S. S. O. Puntodewo, and C. Subarya (2000), Strain partitioning during oblique plate convergence in northern Sumatra: Geodetic and seismologic constraints and numerical modeling, *J. Geophys. Res.*, *105*, 28,363–28,376.

Natawidjaja, D. H., K. Sieh, S. N. Ward, H. Cheng, R. L. Edwards, J. Galetzka, and B. W. Suwargadi (2004), Paleogeodetic records of seismic and aseismic subduction from central Sumatran microatolls, Indonesia, *J. Geophys. Res.*, *109*, B04306, doi:10.1029/2003JB002398.

Newcomb, K. R., and W. R. McCann (1987), Seismic history and seismotectonics of the Sunda Arc, *J. Geophys. Res.*, *92*, 421–439.

Prawirodirdjo, L., Y. Bock, R. McCaffrey, J. Genrich, E. Calais, C. Stevens, S. S. O. Puntodewo, C. Subarya, J. Rais, and P. Zwick (1997), Geodetic observations of interseismic strain segmentation at the Sumatra subduction zone, *Geophys. Res. Lett.*, *24*, 2601–2604.

Reif, C., T. G. Masters, P. Shearer, and G. Laske (2002), Cluster analysis of long period waveforms: Implications for global tomography, *Eos Trans. AGU*, *83*(47), Fall Meet. Suppl., Abstract S51A-1017.

Rivera, L., K. Sieh, D. Helmberger, and D. Natawidjaja (2002), A comparative study of the Sumatran subduction-zone earthquakes of 1935 and 1984, *Bull. Seismol. Soc. Am.*, *92*, 1721–1736.

Sieh, K., S. N. Ward, D. Natawidjaja, and B. W. Suwargadi (1999), Crustal deformation at the Sumatran subduction zone revealed by coral rings, *Geophys. Res. Lett.*, *26*, 3141–3144.

Stein, S., and E. A. Okal (2005), Speed and size of the Sumatra earthquake, *Nature*, *434*, 581–582.

Zachariasen, J., K. Sieh, F. W. Taylor, R. L. Edwards, and W. S. Hantoro (1999), Submergence and uplift associated with the giant 1833 Sumatran subduction earthquake: Evidence from coral microatolls, *J. Geophys. Res.*, *104*, 895–920.

M. Ishii, P. M. Shearer, and K. T. Walker, Institute of Geophysics and Planetary Physics, Scripps Institution of Oceanography, University of California, San Diego, 9500 Gilman Avenue, MC 0225, La Jolla, CA 92093-0225, USA. (walkder@ucsd.edu)